MAGNETIC RESONANCE

CrossMark

Visualization of the lenticulostriate arteries at 3T using black-blood T1-weighted intracranial vessel wall imaging: comparison with 7T TOF-MRA

Zihao Zhang[1,2] • Zhaoyang Fan[3,4] • Qingle Kong[1,5] • Jiayu Xiao[6] • Fang Wu[8] • Jing An[7] • Qi Yang[3,8] • Debiao Li[3,9] • Yan Zhuo[1,2]

Abstract

Objectives The objective of this study was to explore the feasibility of using intracranial T1-weighted vessel wall imaging (VWI) to visualize the lenticulostriate arteries (LSAs) at 3T.

Material and methods Thirteen healthy volunteers were examined with VWI at 3T and TOF-MRA at 7T during the same day. On the vascular skeletons obtained by manual tracing, the number of stems and branches of LSAs were counted. On the most prominent branch in every hemisphere, the contrast-to-noise ratio (CNR), the full length and the local length (5-15 mm above MCAs) were measured and compared between the two methods. Nine stroke patients with intracranial artery stenosis were also recruited into the study. The branches of LSAs were compared between the symptomatic and asymptomatic side.

Results The extracted vascular trees were in good agreement between 7T TOF-MRA and 3T VWI. The two acquisitions showed similar numbers of the LSA stems. The number of branches revealed by 3T VWI was slightly lower than 7T TOF. The full lengths were slightly lower by VWI at 3T ($p = 0.011$, ICC = 0.917). The measured local lengths (5-15 mm from MCAs) showed high coherence between VWI and TOF-MRA ($p = 0.098$, ICC = 0.970). In stroke patients, 12 plaques were identified on MCA segments, and nine plaques were located on the symptomatic side. The average numbers of LSA visualized by 3T VWI were 4.3 ±1.3 on the symptomatic side and 5.0±1.1 on the asymptomatic side.

Conclusion 3T VWI is capable of depicting LSAs, particularly the stems and the proximal segments, with comparable image quality to that of 7T TOF-MRA.

Key Points
• *T1-weighted intracranial VWI at 3T allows for black-blood MR angiography of lenticulostriate artery.*
• *3T intracranial VWI depicts the stems and proximal segments of the lenticulostriate arteries comparable to 7T TOF-MRA.*
• *It is feasible to assess both large vessel wall lesions and lenticulostriate vasculopathy in one scan.*

Zihao Zhang and Zhaoyang Fan contributed equally to this work.

✉ Qi Yang
  yangyangqiqi@gmail.com

1 State Key Laboratory of Brain and Cognitive Science, Institute of Biophysics, Chinese Academy of Sciences, Beijing, China

2 The Innovation Center of Excellence on Brain Science, Chinese Academy of Sciences, Beijing, China

3 Biomedical Imaging Research Institute, Cedars-Sinai Medical Center, Los Angeles, CA 90048, USA

4 Department of Medicine, University of California, Los Angeles, CA, USA

5 University of Chinese Academy of Sciences, Beijing, China

6 Department of Radiology, Chaoyang Hospital, Capital Medical University, Beijing, China

7 Siemens Shenzhen Magnetic Resonance Ltd., Shenzhen, China

8 Department of Radiology, Xuanwu Hospital, Capital Medical University, Beijing, China

9 Departments of Medicine and Bioengineering, University of California, Los Angeles, CA, United States

Abbreviations

3D	Three-dimensional
7T	7 Tesla
CNR	Contrast-to-noise ratio
CR	Contrast ratio
CSF	Cerebrospinal fluid
DSA	Digital subtraction angiography
FSBB	Flow-sensitive black-blood
ICC	Intraclass correlation coefficient
LSA	Lenticulostriate artery
MCA	Middle cerebral artery
MinIP	Minimum intensity projections
MIP	Maximum intensity projections
MPR	Multi-planar reconstruction
MRI	Magnetic resonance imaging
SPACE	Sampling perfection with application-optimized contrast using different flip angle evolutions
T1w	T1-weighted
TOF-MRA	Time-of-flight magnetic resonance angiography
VWI	Vessel wall imaging

Introduction

The lenticulostriate artery (LSA) supplies the blood to the basal ganglia and its vicinity in the brain [1]. Impairment of the LSA is associated with ischemic stroke [2, 3] and small vessel disease [4]. Visualization of the LSA is essential for understanding the mechanisms of microvascular pathologies and potential guiding therapeutic intervention. LSA imaging remains challenging due to the small size of perforating arteries and digital subtraction angiography (DSA) is regarded as a gold standard [5]. However, as an invasive modality mandating the use of potentially nephrotoxic contrast medium and ionizing radiation, DSA is unsuited for repeated imaging or research-oriented studies [5].

Noninvasive imaging of the LSA has recently been feasible with three-dimensional (3D) magnetic resonance imaging (MRI). There are two types of techniques previously investigated, i.e., time-of-flight (TOF) magnetic resonance angiography (MRA) and flow-sensitive black-blood (FSBB) MRI. TOF-MRA of the LSA was initially demonstrated successfully at ultra-high-field 7 Tesla (7T) that allows for bright-blood visualization with superior spatial resolution and vessel-to-tissue contrast [6–9]. The number and length of LSA branches can be quantified and have been associated with some diseases [10–12]. However, the availability of 7T systems is very limited in clinical settings. At clinical field strengths (i.e., 1.5T

or 3T), TOF-MRA integrated with a few quality-enhancing technologies was later shown to be able to quantify the number of LSA stems [13, 14]. Its anisotropic spatial resolution (high in-plane but low slice resolution) might be suboptimal for visualizing smaller distal LSA branches [7]. In contrast, FSBB MRI is a black-blood MRA technique in which the signal of flowing blood is exclusively suppressed and the vascular lumens is depicted with a negative contrast. The success in delineating the LSA with FSBB MRI has been demonstrated at both 1.5T [15] and 3T [16].

Intracranial vessel wall imaging (VWI) shows the similar blood-nulling effect in large cerebral arteries at clinical field strengths. T1-weighted (T1w) 3D turbo spin-echo with variable refocusing flip angles has particularly been advocated as a method of choice for intracranial VWI, given its high spatial resolution and SNR as well as adequate signal suppression of both blood flow and surrounding cerebrospinal fluid (CSF) [17]. All of the features are also, in principle, beneficial for imaging the LSA, an ultra-small structure often surrounded by fluid-containing perivascular spaces [18]. Thus, we hypothesized that the VWI approach at 3T may additionally allow for black-blood angiographic visualization of the LSA. This work was primarily aimed to validate the hypothesis in healthy volunteers using 7T TOF-MRA as a reference standard. Additionally, simultaneous LSA visualization and large-vessel wall evaluation was further explored in patients with a striatocapsular infarction secondary to large vessel atherosclerosis.

Materials and methods

Subjects

Thirteen healthy volunteers (aged 20-37 years, seven males) and nine striatocapsular stroke patients (aged 29-76 years, seven males) with atherosclerotic plaques at the middle cerebral artery (MCA) and ischemic infarctions at the basilar ganglia were enrolled for the study approved by the local institutional review board. Informed consent was obtained from all participants.

Magnetic resonance imaging

All the healthy volunteers were examined with VWI on a 3T system (MAGNETOM Prisma, Siemens Healthineers) and TOF-MRA on a 7T research system (Siemens Healthineers) during the same day. A 64-channel head/neck coil and a 32-channel head coil were used for signal reception at 3T and 7T, respectively. The patients were scanned with VWI at 3T as well.

A recently developed VWI technique was investigated in this study for the feasibility of imaging the LSA at 3T. Briefly, the technique couples a commercially available T1w 3D turbo spin-echo sequence, namely SPACE (Sampling Perfection with Application-optimized Contrast using different flip angle Evolutions), with non-selective excitation and a trailing magnetization flip-down module [19, 20]. VWI of whole-brain large cerebral arteries can be completed with enhanced T1 contrast weighting and CSF-signal suppression.

The imaging parameters for VWI included: sagittal orientation, field of view = 170×170 mm^2, 240 slices, voxel size = 0.53×0.53×0.53 mm^3, TR/TE = 900/13 ms, echo train length = 52, and scan time = 8 min 7 s [19]. The protocol of TOF-MRA at 7T was adapted from Kang et al [7]. A flip angle of 20° was used to meet the radiofrequency safety limit for broader population. Other parameters were: oblique axial orientation, one slab of 40 mm thick, field of view = 180×135 mm^2, voxel size = 0.23×0.23×0.34 mm^3, TR/TE = 15/4.3 ms, and acquisition time = 7 min 34 s.

Image analysis

Images were reviewed and analyzed using commercial software (Osirix MD, Pixmeo SARL).

The healthy subjects with either TOF-MRA or VWI images corrupted by motion artifacts were excluded from analysis. VWI and TOF-MRA images were both reformatted into coronal planes. Consecutive minimum intensity projections (MinIP) were generated for VWI, whereas consecutive maximum intensity projections (MIP) were created for TOF-MRA. A small projection thickness (0.92 mm) was empirically chosen to enhance the confidence of vessel identification and tracing. Using these and the raw images, the LSAs arising from the M1 segment of the MCA were visually identified by an experienced radiologist and then evaluated as follows.

The most prominent branch of the LSAs was identified in each hemisphere. The contrast-to-noise ratio (CNR) between the vessel lumen and surrounding brain tissue was calculated at four locations that are approximately 5, 10, 15, 20 mm above the MCA M1. The CNR was defined as:

$$CNR_{TOF} = \frac{\max(Signal_{lumen}) - \mathrm{mean}(Signal_{tissue})}{\mathrm{std}(Noise)}$$

$$CNR_{VWI} = \frac{\mathrm{mean}(Signal_{tissue}) - \min(Signal_{lumen})}{\mathrm{std}(Noise)}$$

Of note, the maximal/minimal value of the lumen was used to represent the signal of the LSA to avoid the error caused by the inclusion of other tissues in regions-of-interest. Noise was measured at regions with no anatomical structures. All above signal measurements were performed on the consecutive MinIP / MIP images.

Because of the challenges in the automatic modelling of LSAs [21], we built the vascular skeleton by manually tracing the centre lines of the MCAs and LSAs using SimVascular software (http://simvascular.github.io/) [22]. This commercial software package allows for multi-planer reconstruction of images and modelling of vasculatures, and has been used in numerous cardiovascular and neurovascular studies [23–25]. Tracing was manually performed by a radiologist (with 2-year experience in MRI image interpretation) who recursively screened the MinIP/MIP images and delineated the centre points along each visible arterial segment. Tracing continued as long as the contrast ratio (CR) between LSA lumen and adjacent tissue was above 1.3. For TOF-MRA, CR = $Signal_{lumen}/Signal_{tissue}$; For VWI, CR = $Signal_{tissue}/Signal_{lumen}$. The generated skeletons of LSAs were examined by another senior radiologist (with 5-year experience in MRI image interpretation), ensuring the skeletons reflected the centre-lines of the LSAs, and the delineated length was reasonable according to the pre-defined CR criterion. The number of stems, the number of branches, the full length between the origin and the terminal, and the local length (5-15 mm from MCAs) were analyzed in the skeletonized vascular tree. Stems were defined as the LSAs that originated directly from the MCA M1, and branches were defined as daughter vessels originating from the parent LSA stems plus stems without any branches [11]. The full length and the local length (5-15 mm from MCAs) were measured from the most prominent LSA in each hemisphere.

To demonstrate the feasibility of using 3T VWI to simultaneously visualize the LSAs and large-vessel wall, curved multi-planar reconstruction (curved-MPR) was constructed along the MCAs and coronal MinIP (projection thickness = 16 mm) was generated with VWI images in both patients and healthy volunteers.

Statistical analysis

All quantitative data were expressed as means ± standard deviations. The CNR was determined at four pre-defined locations (5 mm, 10 mm, 15 mm and 20 mm above the MCAs). The full lengths and the local length of the most prominent LSA branch acquired by TOF-MRA and VWI were compared using Bland-Altman plotting and a paired-sample t-test. Wilcoxon signed-rank test was used to compare the numbers of stems and branches between the two imaging methods. A p value of less than 0.05 indicated statistical significance. Intraclass correlation coefficient (ICC) was calculated and reported for all the morphological measurements of LSA. All statistical analyses were performed by using commercial software (SPSS 22.0, IBM).

Fig. 1 The 3T VWI (MinIP) and 7T TOF-MRA (MIP) of one volunteer (slab thickness = 20 mm), and their fusion view. The extracted vascular trees show high consistency between TOF-MRA and VWI
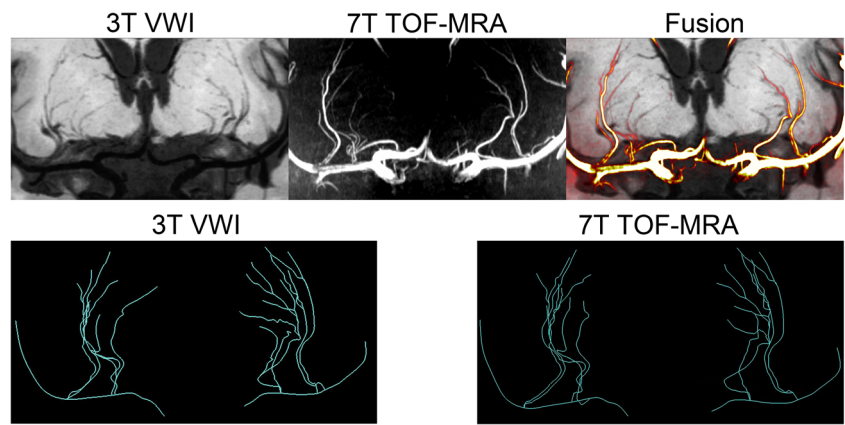
Results

Twelve healthy volunteers were finally included in analysis with acceptable image quality in both 3T VWI and 7T TOF-MRA. Representative MinIPs and MIPs as well as traced vessel skeletons generated from the two methods are shown in Figs. 1 and 2. In general, the traced vessel skeletons of both methods demonstrated similar structures and numbers of LSA stems (Fig. 1). However, in eight of 12 volunteers, 7T TOF-MRA showed more LSA branches (Fig. 2, Table 1).

The lumen-tissue CNRs measured with the two imaging methods are illustrated in Fig. 3. 3T VWI yielded CNR similar to 7T TOF-MRA at the most proximal location (5 mm, $p = 0.206$), but a lightly lower CNR at 10 mm ($p = 0.033$), and significantly lower CNRs at 15 mm ($p = 0.001$), and 20 mm ($p = 0.003$) above the MCA M1.

The numbers of stems and branches of the LSAs are summarized in Table 1. The numbers of stems visualized on 7T TOF-MRA and 3T VWI were comparable (Left: 4.0±1.0 vs. 3.8±1.0, $p = 0.257$, ICC = 0.818; Right: 4.2±0.9 vs. 4.2±1.0, $p = 1.000$, ICC = 0.951). The number of branches visualized by 3T VWI was slightly lower than that by 7T TOF-MRA in most cases, which is statistically significant in the left

hemispheres (Left: 7.7±1.9 vs. 6.7±1.7, $p = 0.031$, ICC = 0.818; Right: 7.9±2.1 vs. 7.3±1.9, $p = 0.057$, ICC = 0.920) (Fig. 4).

The lengths were statistically higher in TOF-MRA than in VWI (47.5±8.3 vs. 45.7±7.7, $p = 0.011$, ICC = 0.917). Bland-Altman plots are shown in Fig. 5a, indicating that TOF-MRA at 7T displayed more distal tiny branches than VWI at 3T. The length was further analyzed by extracting parts of LSAs with vertical distances of 5-15 mm from MCAs. The measurement of local length was consistent between TOF-MRA and VWI (14.9±2.2 vs. 14.7±2.1, $p = 0.098$, ICC = 0.910, Fig. 5b). This result demonstrated that the vasculature visible at 3T VWI was identical to that of 7T TOF-MRA.

For the patients with intracranial atherosclerosis, the coronal MinIP of VWI showed asymmetrical structures of LSA. The numbers of LSA were 4.3±1.3 on the symptomatic side and 5.0±1.1 on the asymptomatic side. The vessel wall lesion was clearly indicated in the curved-MPR along MCAs. In nine patients, nine plaques were identified on MCA-M1 on the symptomatic side, and three plaques were identified on the asymptomatic side. The combined evaluation of LSA vasculatures and large arterial lesions was, therefore, available via a single VWI scanning in about 8 minutes. Figure 6

Fig 2 The 3T VWI (MinIP) and 7T TOF-MRA (MIP) of another volunteer (slab thickness = 20 mm), and their fusion view. The vascular trees show more branches of LSAs revealed in TOF-MRA than VWI, as pointed by the yellow arrowheads
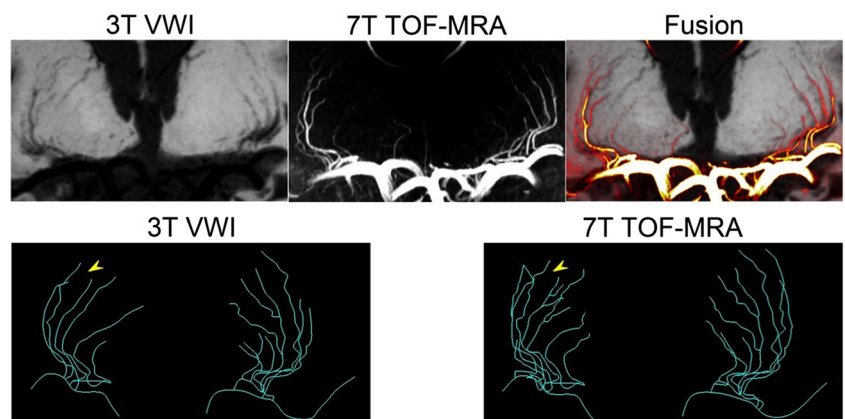
Table 1 The numbers of stems and branches of LSAs visualized by 7T TOF-MRA and 3T VWI, in left and right hemispheres respectively

Subject	Left hemisphere				Right hemisphere			
	Stems		Branches		Stems		Branches	
	TOF-MRA	VWI	TOF-MRA	VWI	TOF-MRA	VWI	TOF-MRA	VWI
S01	2	2	5	4	3	3	6	5
S02	5	4	10	8	5	4	10	8
S03	3	3	7	4	5	5	12	10
S04	5	5	6	6	4	4	6	6
S05	5	5	11	7	5	5	10	10
S06	3	3	9	8	4	4	6	6
S07	4	4	7	6	2	2	6	5
S08	4	3	7	8	4	4	8	9
S09	4	5	10	10	5	5	9	8
S10	5	3	7	6	4	4	9	7
S11	4	4	6	6	4	4	6	5
S12	4	4	7	7	5	6	7	8

demonstrated an example of the vessel wall lesion on MCA and the impaired LSA on the ipsilateral side, compared with a healthy subject.

Discussion

Using a T1w VWI technique, we have obtained detailed black-blood angiographic delineation for the LSAs from normal volunteers, which has been challenging at 3T. We also found in the current study that the LSAs visualized at 3T correlated well with that from 7T TOF-MRA. In some cases (S08, S09 and S12), VWI revealed more branches or stems

Fig. 3 The CNR of lumens to tissues measured in the images of 3T VWI and 7T TOF-MRA

than TOF-MRA, which may be attributed to the deficient signal enhancement in small vessels with slow blood flow velocity by TOF-MRA. Our results suggest that T1w VWI is a promising technique for imaging the LSAs.

LSAs branching from the MCA are major feeding arteries for the corpus striatum in the sub-cortex and extremely important for ensuring regular brain supply. These small vessels can be implicated in deep brain infarctions and small vessel diseases such as vascular dementia [2–4]. Assessment of LSA patency may provide important information on risk stratification and treatment response. For example, fewer LSA stems and branches have been correlated to hypertension, a major risk factor for microvascular injury [11]. Serial monitoring for the number and length of small vessels in hypertensive patients would be useful to predict the risk of lacunar infarctions and may allow more preventive interventions. Kang et al reported that the LSAs in patients with basal ganglia infarcts were significantly less than normal controls [10]. In concordance with their study, we found in our study that the number of LSAs was lower on the symptomatic side versus the asymptomatic side (4.3 ± 1.3 vs 5.0 ± 1.1), highly suggesting occlusion of the LSAs as a direct cause. Detailed assessment of the number and length of the LSAs in a symptomatic patient would help determine the risk of a second stroke in the asymptomatic side. Longitudinal quantification of these metrics may also provide an imaging marker for the effectiveness of secondary prevention treatment.

It has been commonly accepted that 7T TOF-MRA is the currently the state of the art technique for visualization of such small perforating arteries [7]. However, the limited availability of 7T MRI systems hindered its clinical usage. The 3T TOF-MRA is mainly used for large artery imaging and assessing
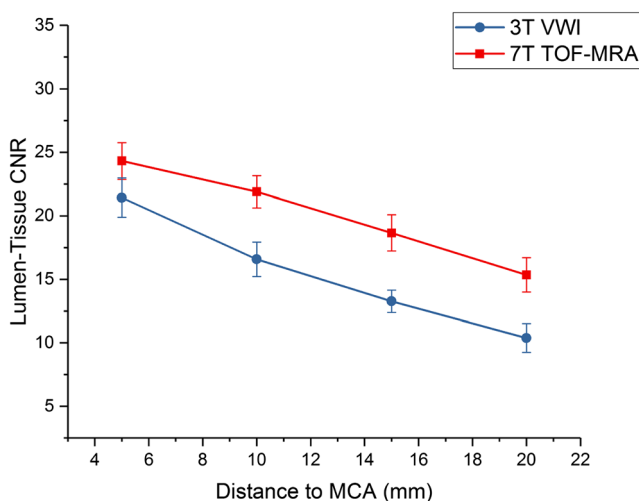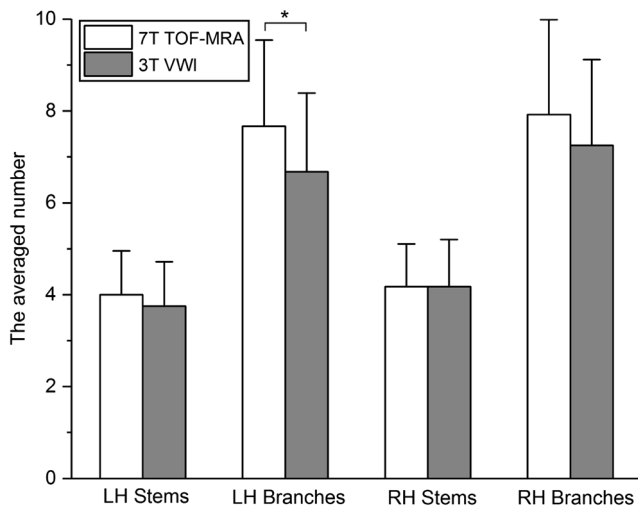
Fig. 4 The stems and branches of LSAs visualized by 7T TOF-MRA and 3T VWI

micro-vasculature still suffers from insufficient imaging resolution and poor SNR. In our study, we proposed a novel VWI-based angiographic method which enables fast and clear visualization of perforating arteries. Of note, the numbers of stems and local length of LSAs visualized by TOF-MRA and VWI showed no significant difference, demonstrating comparable abilities of the two methods on displaying primary structures of LSAs. The lower number of branches may be due to the relatively lower CNR in VWI at 3T. The disagreement in full lengths may be attributed to the uncertainty in vascular tracing in distal areas by 3T VWI (Fig. 2).

The proposed VWI technique shares a similar mechanism, i.e., black-blood angiography, with previously proposed FSBB technique. FSBB has demonstrated significantly better delineation of LSA branches than TOF-MRA at 3T [16], presumably due to its superior sensitivity to low-velocity blood flow, inflow-independent property, and isotropic spatial resolution. VWI inherently possesses these features as well. In previous studies, the average numbers and lengths of

visualized LSAs by FSBB technique were 3.6 and 21.8 mm respectively. In our study, we reported more stems and longer lengths compared with these studies [15, 16]. This is likely due to the limited SNR with GRE based FSBB and its incomplete flow suppression in distal LSAs, when compared to VWI that is based on a high-SNR TSE acquisition. In addition, the intrinsic black-blood effect of TSE enables superior suppression of low-velocity blood flow. To the best of our knowledge, this is the first study using relatively high isotropic spatial resolution (0.53 mm) for LSA imaging at 3T.

Another contributor to the success of VWI with respect to LSA visualization is the strong T1 contrast weighting with CSF suppression. The LSA is known to often be surrounded by fluid-containing perivascular spaces [18]. According to our experience in T2-weighted VWI, perivascular spaces are typically of moderate to high signal intensity and thus overshadow the dark lumen of the LSAs, making it challenging to visualize the LSAs (Supplemental Fig. 1). In contrast, the previously optimized T1w VWI technique by Fan et al has demonstrated considerably enhanced signal suppression of the CSF, although it is not as dark as the vessel lumen [19]. With this technique, the perivascular fluid thus has a negligible detrimental effect on the delineation of the LSAs.

In this work, intracranial VWI was demonstrated as a 2-in-1 approach to imaging of both large-vessel wall and LSA lumen. This feature has not been demonstrated for other techniques including FSBB that has limited SNR for visualizing large-vessel wall. VWI has been widely used for direct characterization of vessel wall lesions in large cerebral vessels [17]. The additional capacity of depicting the perforating arteries enables the technique more powerful for studying the mechanism of deep subcortical infarctions and small vessel disease. It has been postulated that striatocapsular infarctions result from occlusion of the proximal perforating arteries by atherosclerotic plaques at the parent large vessels [26]. Using high resolution MRI, Yoon et al reported that superior MCA wall plaques near the orifice of LSAs were more likely to be
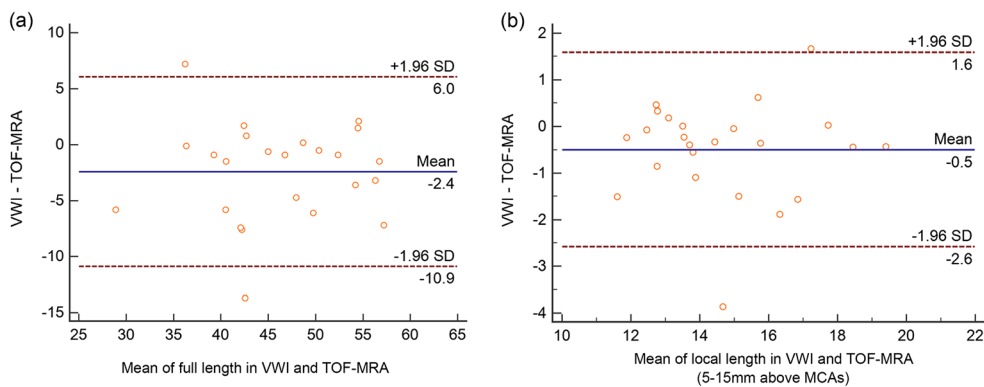

Fig. 5 Bland-Altman plots represent the differences of (**a**) full lengths measured in the predominant vascular trees of TOF-MRA and VWI. The visible structures of predominant arteries were completely evaluated. **b**

The lengths of predominant arteries with 5-15 mm vertical distance from MCAs were consistent in TOF-MRA and VWI, confirming the uniform vasculature imaged by the two methods.
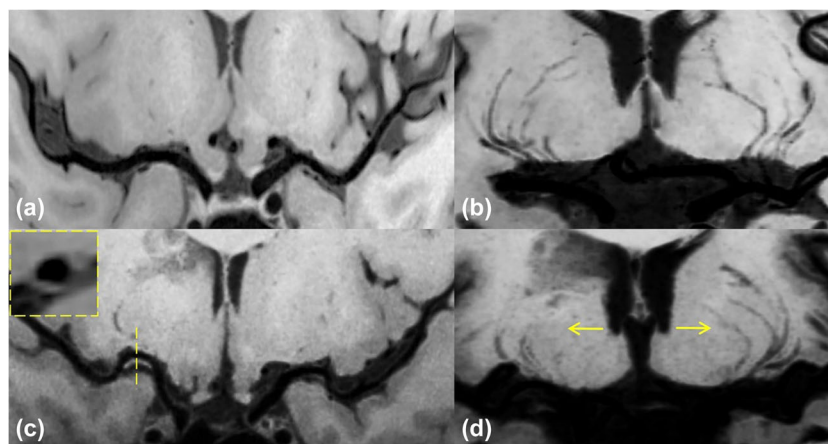
Fig. 6 The reconstructed images of a 37-year-old female healthy volunteer (**a,b**) and a 62-year-old female with an acute infarction in right basal ganglia (**c,d**). **a** The curved-MPR showed no thickening of MCA wall in both sides. **b** Coronal MinIP revealed symmetrical LSAs of the left and right hemispheres. **c** The curved-MPR showed a plaque with hyperintensity (yellow line) on the MCA wall. **d** Coronal MinIP revealed decrease of right LSA branches compared to the left side (yellow arrow)

symptomatic, resulting in larger penetrating artery infarction [27]. The proposed T1w VWI technique will simultaneously unravel large-vessel wall pathologies and small-vessel patency, which helps understand the causal relation between them. This will open the door to further investigations such as the effect of circumferential distribution and burden of parent vessel atherosclerosis on the incidence or progression of small vessel occlusion, which is substantially meaningful for primary and secondary stroke prevention. We believe these potential benefits may also apply to lacunar infarction and small vessel diseases whereby correlation or causal relation to the large-vessel atherosclerosis has drawn great interest. It is also noteworthy that the spatial relation between LSAs and brain lesions (e.g., enhancing recent infarcts or hypointense chronic infarcts) can be easily understood by using VWI.

However, VWI still has some disadvantages that need to be overcome in the future. Firstly, vascular tracing in VWI images was performed using MinIP images. The perivascular space or CSF might possibly be detected as the same signal void as LSAs. However, detected LSAs using MiniIP showed consistent geometry as 7T TOF MRA, which is not affected by perivascular spaces and CSF. Secondly, the contrast of the lumen to the surrounding tissue may be insufficient for identifying the far end of the LSA using 3T VWI. Some tiny extremities are therefore not confidently visible in the images. Finally, VWI shows good contrast between vessels and parenchyma, but it is yet unknown whether this technique is effective to show lesions in small arteries.

There are several limitations in our study. Firstly, we did not compare TOF-MRA and VWI at 3T. The main goal of this study was to show proof-of-concept on the ability of using 3T VWI for visualizing the LSAs. Assessment of the ability is better achieved through a validation against a well-accepted or best-available reference, which is 7T TOF-MRA [6, 7]. Secondly, we chose 7T TOF-MRA instead of DSA as a reference for evaluating the imaging quality of LSAs visualization. Although DSA is considered the "gold standard" method, its invasiveness hinders its application on healthy volunteers. In addition, it is difficult to track LSA branches on routine DSA, due to faint filling of LSA branches and disturbance of other vascular branches causing unclean background. Head to head comparison with VWI is also hard to achieve because of the different imaging techniques. Lastly, our study was a preliminary study that included relatively a small number of samples. The fidelity of using VWI at 3T for imaging LSAs should be evaluated in a larger population in the future. Advanced automatic segmentation and reconstruction of LSAs should be introduced to facilitate the image post-processing and provide an objective measurement of arterioles.

In conclusion, we demonstrated that VWI is a credible technique for angiographic delineation of the LSAs at a clinical available 3T MR system. The simultaneously obtained LSA angiography and VWI of large vessels will greatly facilitate the etiological study of intracranial atherosclerosis and ischemic stroke.

Compliance with ethical standards

Guarantor The scientific guarantor of this publication is Qi Yang.

Conflict of interest Dr. Jing An is an employee of Siemens Shenzhen Magnetic Resonance Ltd. Other authors of this manuscript declare no

relationships with any companies, whose products or services may be related to the subject matter of the article.

Statistics and biometry   Zhuang Tao kindly provided statistical advice for this manuscript.

Informed consent   Written informed consent was obtained from all subjects (patients) in this study.

Ethical approval   Institutional Review Board approval was obtained.

Methodology
• prospective
• observational
• performed at one institution

References

1. Marinković S, Gibo H, Milisavljević M, Ćetković M (2001) Anatomic and clinical correlations of the lenticulostriate arteries. Clin Anat 14:190–195. https://doi.org/10.1002/ca.1032

2. Greenberg SM (2006) Small vessels, big problems. N Engl J Med 354:1451–1453. https://doi.org/10.1056/NEJMp068043

3. Feekes JA, Hsu SW, Chaloupka JC, Cassell MD (2005) Tertiary microvascular territories define lacunar infarcts in the basal ganglia. Ann Neurol 58:18–30. https://doi.org/10.1002/ana.20505

4. Román GC, Erkinjuntti T, Wallin A, Pantoni L, Chui HC (2002) Subcortical ischaemic vascular dementia subcortical ischaemic vascular dementia. Lancet Neurol 1:426–436. https://doi.org/10.1016/S1474-4422(02)00190-4

5. Tanriover N, Kawashima M, Rhoton AL Jr, Ulm AJ, Mericle RA (2003) Microsurgical anatomy of the early branches of the middle cerebral artery: morphometric analysis and classification with angiographic correlation. J Neurosurg 98:1277–1290. https://doi.org/10.3171/jns.2003.98.6.1277

6. Cho ZH, Kang CK, Han JY et al (2008) Observation of the lenticulostriate arteries in the human brain in vivo using 7.0T MR angiography. Stroke 39:1604–1606. https://doi.org/10.1161/STROKEAHA.107.508002

7. Kang CK, Park CW, Han JY et al (2009) Imaging and analysis of lenticulostriate arteries using 7.0-Tesla magnetic resonance angiography. Magn Reson Med 61:136–144. https://doi.org/10.1002/mrm.21786

8. Hendrikse J, Zwanenburg JJ, Visser F, Takahara T, Luijten P (2008) Noninvasive depiction of the lenticulostriate arteries with time-of-flight MR angiography at 7.0 T. Cerebrovasc Dis 26:624–629. https://doi.org/10.1159/000166838

9. von Morze C, Xu D, Purcell DD et al (2007) Intracranial time-of-flight MR angiography at 7T with comparison to 3T. J Magn Reson Imaging 26:900–904. https://doi.org/10.1002/jmri.21097

10. Kang CK, Park CA, Park CW, Lee YB, Cho ZH, Kim YB (2010) Lenticulostriate arteries in chronic stroke patients visualised by 7 T magnetic resonance angiography. Int J Stroke 5:374–380. https://doi.org/10.1111/j.1747-4949.2010.00464.x

11. Kang CK, Park CA, Lee H et al (2009) Hypertension correlates with lenticulostriate arteries visualized by 7T magnetic resonance angiography. Hypertension 54:1050–1056. https://doi.org/10.1161/HYPERTENSIONAHA.109.140350

12. Seo SW, Kang CK, Kim SH et al (2012) Measurements of lenticulostriate arteries using 7T MRI: new imaging markers for subcortical vascular dementia. J Neurol Sci 322:200–205. https://doi.org/10.1016/j.jns.2012.05.032

13. Chen YC, Li MH, Li YH, Qiao RH (2011) Analysis of correlation between the number of lenticulostriate arteries and hypertension based on high-resolution MR angiography findings. AJNR Am J Neuroradiol 32:1899–1903. https://doi.org/10.3174/ajnr.A2667

14. Chen YC, Li YH, Lu J, Li WB, Wang JB (2016) Correlation between the reduction in lenticulostriate arteries caused by hypertension and changes in brain metabolism detected with MRI. AJR Am J Roentgenol 206:395–400. https://doi.org/10.2214/AJR.15.14514

15. Gotoh K, Okada T, Miki Y et al (2009) Visualization of the lenticulostriate artery with flow-sensitive black-blood acquisition in comparison with time-of-flight MR angiography. J Magn Reson Imaging 29:65–69. https://doi.org/10.1002/jmri.21626

16. Okuchi S, Okada T, Fujimoto K et al (2014) Visualization of Lenticulostriate Arteries at 3T: Optimization of Slice-selective off-resonance Sinc Pulse-prepared TOF-MRA and its comparison with flow-sensitive black-blood MRA. Acad Radiol 21:812–816. https://doi.org/10.1016/j.acra.2014.03.007

17. Mandell DM, Mossa-Basha M, Qiao Y et al (2017) Intracranial vessel wall MRI: principles and expert consensus recommendations of the American Society of Neuroradiology. AJNR Am J Neuroradiol 38:218–229. https://doi.org/10.3174/ajnr.A4893

18. Wardlaw JM, Smith C, Dichgans M (2013) Mechanisms of sporadic cerebral small vessel disease: insights from neuroimaging. Lancet Neurol 12:483–497. https://doi.org/10.1016/S1474-4422(13)70060-7

19. Fan Z, Yang Q, Deng Z et al (2017) Whole-brain intracranial vessel wall imaging at 3 Tesla using cerebrospinal fluid–attenuated T1-weighted 3D turbo spin echo. Magn Reson Med 77:1142–1150. https://doi.org/10.1002/mrm.26201

20. Yang Q, Deng Z, Bi X et al (2017) Whole-brain vessel wall MRI: a parameter tune-up solution to improve the scan efficiency of three-dimensional variable flip-angle turbo spin-echo. J Magn Reson Imaging 46:751–757. https://doi.org/10.1002/jmri.25611

21. Liao W, Rohr K, Kang C-K, Cho Z-H, Wörz S(2016) Automatic 3D segmentation and quantification of lenticulostriate arteries from high-resolution 7 tesla MRA images. IEEE Trans Image Process 25:400–413. https://doi.org/10.1109/TIP.2015.2499085

22. Updegrove A, Wilson NM, Merkow J, Lan H, Marsden AL, Shadden SC (2017) SimVascular: an open source pipeline for cardiovascular simulation. Ann Biomed Eng 45:525–541. https://doi.org/10.1007/s10439-016-1762-8

23. Sengupta D, Kahn AM, Burns JC, Sankaran S, Shadden SC, Marsden AL (2012) Image-based modeling of hemodynamics in coronary artery aneurysms caused by Kawasaki disease. Biomech Model Mechanobiol 11:915–932. https://doi.org/10.1007/s10237-011-0361-8

24. Mukherjee D, Padilla J, Shadden SC (2016) Numerical investigation of fluid–particle interactions for embolic stroke. Theor Comput Fluid Dyn 30:23–39. https://doi.org/10.1007/s00162-015-0359-4

25. Mukherjee D, Jani ND, Selvaganesan K, Weng CL, Shadden SC (2016) Computational assessment of the relation between embolism source and embolus distribution to the circle of Willis for improved understanding of stroke etiology. J Biomech Eng 138:081008. https://doi.org/10.1115/1.4033986

26. Yamamoto Y, Ohara T, Hamanaka M, Hosomi A, Tamura A, Akiguchi I (2011) Characteristics of intracranial branch atheromatous disease and its association with progressive motor deficits. J Neurol Sci 304:78–82. https://doi.org/10.1016/j.jns.2011.02.006

27. Yoon Y, Lee DH, Kang DW, Kwon SU, Kim JS (2013) Single subcortical infarction and atherosclerotic plaques in the middle cerebral artery. Stroke 44:2462–2467. https://doi.org/10.1161/STROKEAHA.113.001467